Nanopowder synthesis enabling 1350 ºC full densification of $(Gd,La)_2O_2S:Pr^{3+}$ luminescent ceramics via pressureless sintering and the effect of La^{3+} doping

Zhenqi Song[a], Fan Li[a], Sihan Feng[a], Zhiyuan Pan[a], Xuejiao Wang[b], Qi Zhu[a,*], Ji-Guang Li[c,*]

[a] *Key Laboratory for Anisotropy and Texture of Materials, School of Materials Science and Engineering, Northeastern University, Shenyang, Liaoning 110819, China*

[b] *College of Chemistry and Materials Engineering, Bohai University, Jinzhou, Liaoning 121007, China*

[c] *Research Center for Electronic and Optical Materials, National Institute for Materials Science, Tsukuba, Ibaraki 305-0044, Japan*

[*]Corresponding author
Prof. Qi Zhu
Northeastern University
E-mail: zhuq@neu.edu.cn
Tel: +86-24-83672700

Dr. Ji-Guang Li
National Institute for Materials Science
E-mail: li.jiguang@nims.go.jp
Tel: +81-29-860-4394

Abstract

Pr^{3+} activated Gd_2O_2S ($Gd_2O_2S:Pr^{3+}$) ceramics are important scintillators for X-ray computed tomography, whose fabrication generally requires harsh sintering conditions, such as 1650-1750 °C for pressureless sintering and ~1300-1500 °C and tens to hundreds MPa for pressure assisted sintering. We synthesized in this work a series of $[(Gd_{1-x}La_x)_{0.99}Pr_{0.01}]_2O_2S$ (GLOS:Pr^{3+}; x=0, 0,15, 0.3, 0.5, 0.65, 0.8, 1.0) nanopowders of fine crystallite size (~19-54 nm), high specific surface area (~13.4-15.8 m^2/g) and unimodal size distribution through two-step calcination of coprecipitated amorphous precursors. Dilatometry analysis confirmed that the nanopowders possess excellent sinterability, and fully dense GLOS:Pr^{3+} ceramics were successfully fabricated via pressureless sintering in an Ar/H_2 gas mixture at a temperature as low as 1350 °C. La^{3+} doping was found to substantially enhance densification/grain growth and the $^3P_0$-$^3H_4$ main emission (~510 nm) of Pr^{3+}, and tends to elongate the fluorescence lifetime of the Pr^{3+} emission (~1.89-2.66 μs).

Keywords: $(Gd,La)_2O_2S:Pr^{3+}$ ceramics; La^{3+} doping; Sintering; Photoluminescence

1. Introduction

Scintillators are capable of converting high-energy rays or particles into ultraviolet or visible light and are widely used in high-energy physics, non-destructive security inspection, medical imaging and other radiation detection applications [1-3]. In recent years, the rapid development of X-ray computed tomography (CT) scanning equipment requires its internal scintillator to have high light output, low afterglow, high X-ray absorption and other properties [4]. As an excellent host material, Gd_2O_2S possesses the advantages of a wide band gap (~4.6-4.8 eV), low phonon energy (~520 cm^{-1}), high X-ray blocking ability (D_{th}=7.34 g/cm^3; Z=64) and excellent thermal/chemical stability [5]. The Pr^{3+} doped into the Gd_2O_2S host as a luminescence center has a high light yield (~35,000 photons/MeV), fast fluorescence decay (lifetime ~2-5 μs) and low afterglow (<0.1% after 3 ms), and the emission peak of the $^3P_0 \rightarrow {}^3H_4$ transition of Pr^{3+}, located near 510 nm, coincides well with the sensitive region of the detector [6-9]. Therefore, $Gd_2O_2S:Pr^{3+}$ ceramics are widely used in CT equipment. Ce^{3+} is sometimes added as a co-dopant because it can reduce the afterglow of Pr^{3+} [7] and improve the resistance to radiative damage [3], though the light output of the ceramic is negatively affected due to the trapping of holes by Ce^{3+} in a non-radiatively bound form [10].

The key to the fabrication of high-performance scintillator ceramics is the preparation of powders, and the conventional method for oxysulfide synthesis is flux reaction at 1200-1300 °C [11,12]. Although the powder produced by this method possesses a high degree of crystallinity, the sintering activity is poor because of its large particle size. The other synthesis methods such as gas-phase sulfurization [13,14], urea-

based precipitation using SO_2/SO_4^{2-} as sulfuration agent [15], self-propagating high-temperature synthesis with thoria [16,17], and thermal cleavage of S-containing chelates in high melting point organic solvents [18] may produce smaller particles, but it is difficult to control phase purity/chemical purity because the affinity of S toward rare earth (RE) elements is much lower than that of the O element. Additionally, all the above powder synthesis methods unavoidably use and/or emit toxic substances.

The sintering techniques for GOS-based ceramics include vacuum hot pressing (HP) [19,20], hot isostatic pressing (HIP) [21,22] , pressureless sintering in vacuum or an atmosphere of argon, nitrogen, or hydrogen [10,23], and spark plasma sintering (SPS) [24], but all require harsh conditions due to the high melting point of the material (~2200 °C) and low powder activity. Despite the addition of sintering aids such as LiF [19] and Li_2GeF_6 [20], HIP, HP and SPS still require high temperatures of ~1300-1500 °C, high pressure (several tens to hundreds MPa) and several hours of holding [19-22,24], while pressureless sintering generally requires ~1650-1750°C [10,23]. These make GOS susceptible to volatilization of the S element and even the formation of an oxide layer on ceramic surface. The loss of S produces vacancies, which hinder the densification process, lower the light output and produce afterglow. Annealing in H_2S gas after sintering may eliminate sulfur vacancies [21,25], but the procedure is complicated and it does not fundamentally solve the problem of S volatilization.

We have two proposals to suppress and even eliminate the S loss during sintering. One is strengthening the RE-S bond through materials design, such as doping GOS with La^{3+} to form (Gd,La)OS solid solutions (GLOS). The idea came from the fact that the

strength of RE-S bond is closely related to the type of RE, and it increases with increasing ionic radius/decreasing electronegativity of RE^{3+} [18,26,27]. In addition, the melting point of La_2O_2S is about 200 ºC lower than that of Gd_2O_2S [28], so it is possible to lower the densification temperature by La^{3+} doping. The other one is lowering the densification temperature through synthesizing powders of higher sintering activity.

We recently reported a pollution-free protocol for the synthesis of (Gd,La)OS:Tb^{3+} solid-solution nanopowders, which involves titration of a mixed solution of RE nitrates and ammonium sulfate with ammonia water at ice-water temperature to obtain a $RE_2(OH)_{4-2m}(CO_3)_m(SO_4)\cdot nH_2O$ (m<1.0) type amorphous precursor, followed by annealing in air to yield a $RE_2O_2SO_4$ intermediate and then in hydrogen to produce RE_2O_2S [5]. Through this technical route, we obtained in this work a series of $[(Gd_{1-x}La_x)_{0.99}Pr_{0.01}]_2O_2S$ (GLOS:Pr^{3+}) solid-solution nanopowders of fine crystallite size, high specific surface area, unimodal size distribution and high sinterability. It was demonstrated that fully densified GLOS:Pr^{3+} ceramics can be fabricated by pressureless sintering in a stream of H_2/Ar gas mixture at the very low temperature of 1350 ºC. The influence of La content on sintering, microstructure, and photoluminescence of the ceramics were also studied in detail.

2. Experimental section

2.1. Powders synthesis and ceramics fabrication

The series of $[(Gd_{1-x}La_x)_{0.99}Pr_{0.01}]_2O_2S$ nanopowders (GLOS:Pr^{3+}; x=0, 0.15, 0.3, 0.5, 0.65, 0.8 and 1.0) were synthesized by calcining coprecipitated precursors [5], which was briefed below. The starting Gd_2O_3, La_2O_3, and Pr_6O_{11} powders (99.99% pure,

Huizhou Ruier Rare Earth High-Tech Co. Ltd., Huizhou, China) were separately dissolved with nitric acid (analytical grade, Sinopharm Chemical Reagent Co., Ltd.) to make nitrate solutions. A mixed solution (300 mL) containing 30 mmol of (La, Gd, $Pr)^{3+}$ and 45 mmol of $(NH_4)_2SO_4$ (Sinopharm Chemical Reagent, Shanghai, China) were then made according to the aforesaid La/Gd/Pr molar ratio, followed by cooling to ~4 ºC, titration with ammonium water (Sinopharm) to pH = 9 under magnetic stirring and homogenization at ~4 ºC for 1 h. The precipitate, recovered by centrifugation, was washed three times with water and once with anhydrous ethanol and then dried in an air oven at 60 °C for 24 h to obtain the precursor. The precursor powder, lightly crushed with a mortar and pestle, was first calcined in air at 950 °C for 2 h to burn off organic molecules and to produce an oxysulfate intermediate phase [5], and then calcined in flowing H_2 gas (100 mL/min) at the same temperature for 2 h to produce GLOS:Pr^{3+} nanopowder, where a heating rate of 5 ºC/min was used for the rising phase of calcination. GLOS:Pr^{3+} ceramics were fabricated by sintering green bodies, cold isostatically consolidated under 300 MPa, at various selected temperatures (1100-1400 °C) for 4 h in a stream of 5 vol%H_2/95 vol% Ar gas mixture (200 mL/min), using a heating rate of 5 °C/min for the ramp stage.

2.2. Characterization techniques

Phase identification of the product was performed by X-ray diffractometry (XRD; Model SmartLab, Rigaku, Tokyo, Japan), using nickel-filtered Cu K_α radiation as the X-ray source (λ = 0.15405 nm) and a scanning rate of 10° 2θ/min. The microstructures of the powders and ceramics were analyzed by field emission scanning electron

microscopy (FE-SEM, Model JSM-7001F, JEOL, Tokyo). The specific surface area of the powder was measured by the Brunauer–Emmett–Teller method (BET; Model TriStar II 3020, Micromeritics, GA, USA) via nitrogen adsorption at 77 K. Particle sizing was conducted with a laser diffraction particle sizer (Model Mastersizer 3000, Malvern, UK), and the suspension for analysis was prepared by ultrasonic dispersion of 2.5 mg powder in 20 mL ethanol.

Dilatometry analysis of the green body was conducted with a Model SETSYS18/24 system (Sataram Instrument Co. Ltd., Lyon, France) with a heating rate of 10 ºC/min in following N_2 gas (200 mL/min). The instantaneous relative density (ρ) of the powder compact can be assayed from the initial value (ρ_0) and the measured linear shrinkage ($\Delta L/L_0$) through the following equation:

$$\rho = \rho_0/(1-\Delta L/L_0)^3 \qquad (1)$$

The relative density of the ceramic fabricated by ramp and holding sintering was measured by the Archimedes method, using deionized water as an intrusion medium. The average grain size of the ceramic was derived by counting at least 200 grains from the as-sintered ceramic surface with the Image-Pro plus V6.0 software (Media Cybernetics, Inc., Washington D. C., USA).

The photoluminescence spectra of the ceramics were recorded at room temperature using an FP-8600 fluorescence spectrophotometer (JASCO, Tokyo) equipped with a Φ60-mm integrating sphere (Model ISF-834, JASCO) and a 150 W Xe-lamp for excitation, and all the measurements were conducted at a scan speed of 100 nm/min and a slit width of 5 nm. The spectral response of the spectrophotometer

was calibrated with an ethylene glycol solution of Rhodamine B (5.5 g/L) and a standard light source unit (ECS-333, JASCO) for the ranges of 220-600 and 350-850 nm, respectively. The fluorescence decay curve of Pr^{3+} was recorded with a DeltaFlex modular fluorescence lifetime testing system (Horiba Scientific, Jobin Yvon IBH Ltd., Scotland), using NanoLED-250 as the excitation source (λ_{em} = 249 nm, 1.2 ns pulse duration).

3. Results and discussion

3.1. Characterization of the powders

The as-dried precursors are all amorphous to X-rays, as found in our previous study [5]. Fig. 1 shows the XRD patterns of the GLOS:Pr^{3+} powders obtained by calcination in H_2 at 950 ºC, where it can be seen that, in each case, the diffraction peaks are well indexable with those of the hexagonal structured Gd_2O_2S (JCPDS No. 26-1422) and La_2O_2S (JCPDS No. 27-0263) and the peaks were gradually shifted toward lower diffraction angles by the lattice expansion induced by the replacement of smaller Gd^{3+} with larger La^{3+} (1.10 Å for La^{3+} and 1.00 Å for Gd^{3+} under 7-fold coordination [29]). Broadening analysis of the XRD peaks using Scherrer formula yielded average grain sizes of ~18.6, 24.6, 25.1, 26.8, 28.9, 31.0, and 53.8 nm for the x = 0, 0.15, 0.3, 0.5, 0,65, 0.8 and 1.0 powders, respectively. Fig. 2 shows the FE-SEM images of three typical precursors and their GLOS:Pr^{3+} derivatives, from which it can be seen that all the products are loose agglomerates of rounded nanoparticles.

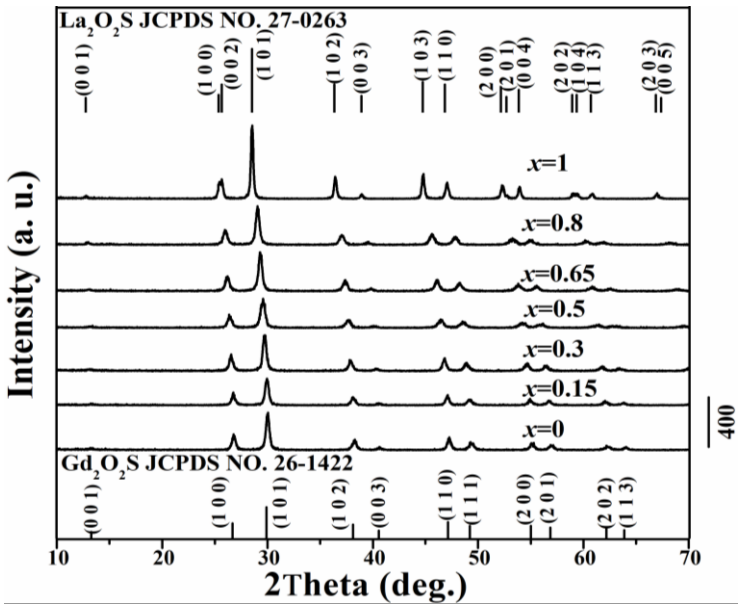

Fig. 1. XRD patterns of the GLOS:Pr^{3+} powders calcined at 950°C in H_2.

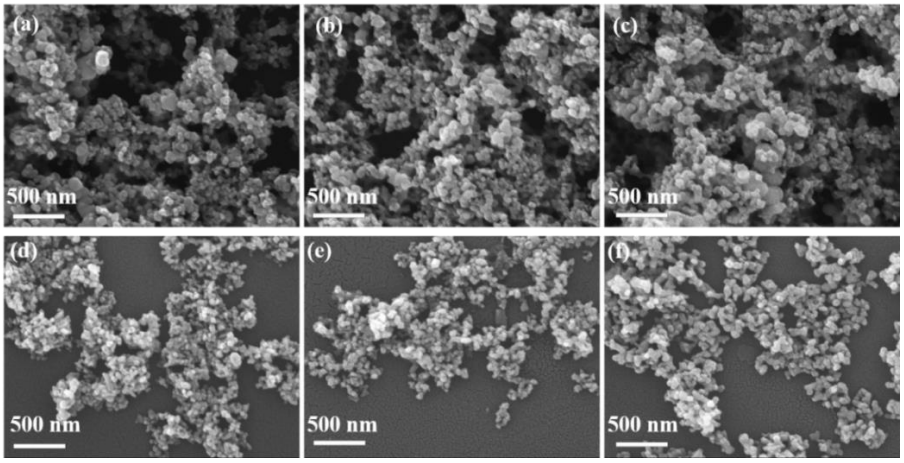

Fig. 2. FE-SEM micrographs of three typical precursor (a, b, c) and GLOS:Pr^{3+}(d, e, f) powders, with x = 0 for (a) and (d), x = 0.5 for (b) and (e), and x = 1.0 for (c) and (f).

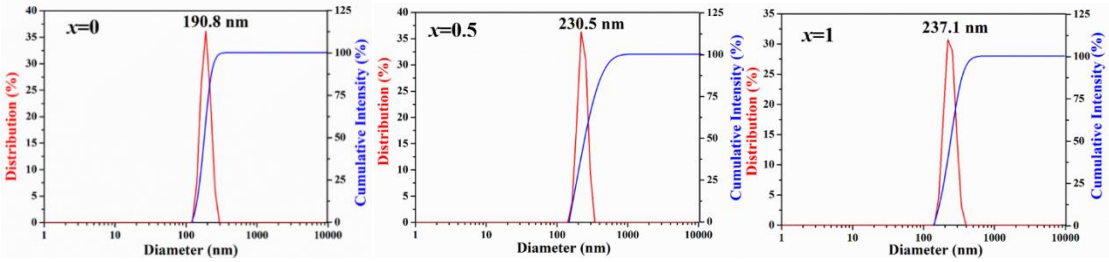

Fig. 3. Particle-size distributions for the three typical GLOS:Pr^{3+}powders of x = 0, 0.5 and 1.0.

Laser diffraction particle sizing confirmed that the three representative powders all have a single-peak size distribution in each case (Fig. 3). The particles were distributed in the ranges of ~120-295, 140-340 and 125-360 nm, with center sizes of ~191, 231,

and 237 nm for x = 0, 0.5 and 1.0, respectively. Such size distributions would be beneficial to the fabrication of uniform phosphor screens for scintillation and cathodoluminescence and to the sintering of high-quality ceramic scintillators. The BET analysis revealed that the specific surface areas of the x = 0, 0.5, and 1.0 powders are about 13.4, 14.5, and 15.8 m^2/g, respectively. The sphere-equivalent particle size D (nm) of the powder can then be derived via equation $D = 6000/(S_{BET} \times \rho)$, where ρ is the theoretical density (g/m^3) of the material, to be ~61 nm for x = 0 , 64 nm for x = 0.5 and 66 nm for x = 1.0.

3.2 Sintering behavior and characterization of GLOS:Pr^{3+} ceramics

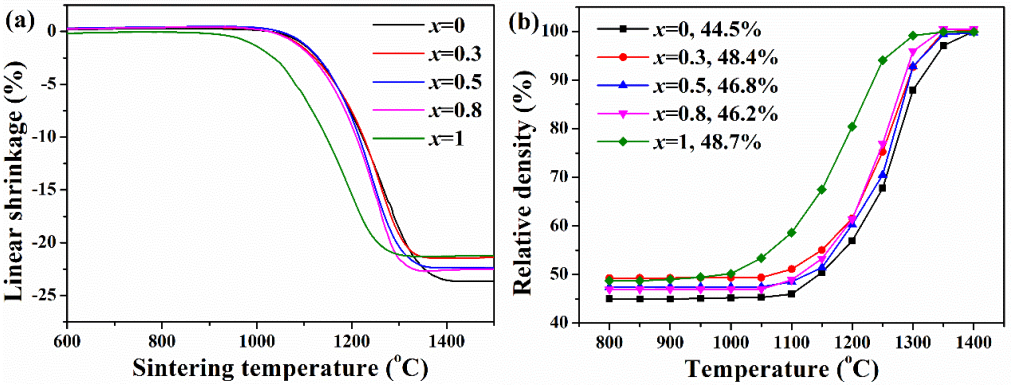

Fig. 4. Line shrinkage (a) and evolution of relative density (b) as a function of temperature for typical GLOS:Pr^{3+} samples.

Fig. 4 shows the results of dilatometry for the five samples of x=0, 0.3, 0.5, 0.8 and 1.0, which were analyzed under a constant heating rate of 10 ºC/min. It is clear that the GLOS:Pr^{3+} powders synthesized in this work possess excellent sinterability and can be sintered to over 99% of the theoretical density at the low temperature of 1400 ºC without holding time (Fig. 4b), with the onset temperature of rapid sintering being as low as ~1100 °C (Fig. 4a). This is benefited from the fine crystallite size, low agglomeration, and the unimodel and narrow size distribution of the particles.

Noteworthy is that the ending temperature of shrinkage became successively lower with increasing La^{3+} content, and this is especially significant for the x = 1.0 sample despite that this composition has the largest initial crystallite size (~54 nm) across the series. This phenomenon could possibly be due to (1) changed character of the chemical bonds, since the ionicity of RE-(O,S) would increase with increasing La^{3+} incorporation by the lower electronegativity of La, and/or (2) faster mass transfer by the lattice expansion induced by La^{3+} doping, which simultaneously promotes sintering and grain growth. This latter case may also account for the gradually larger average crystallize size at the same temperature of powder calcination with increasing La content.

Based on the results of dilatometry, the sintering of ceramics was performed at the six different temperatures of 1100, 1200, 1250, 1300 and 1350 ºC, with a residence time of 4 h in each case. Fig 5a shows the XRD patterns of the series of GLOS:Pr^{3+} ceramics sintered at the highest temperature of 1350 °C, from which it can be confirmed that the products are phase-pure oxysulfide in each case. The ceramics showed much sharper diffractions than the starting powders (Fig. 1), indicating substantial grain growth occurred during sintering. Analyzing the XRD spectra with the Jade 6 software found that lattice constants a ($a = b$) and c and cell volume V increase while theoretical density decreases almost linearly with increasing x value, conforming to the solid-solution nature of the materials. The end composition $La_2O_2S:Pr^{3+}$ (x = 1.0) still has a theoretical density as high as 5.77 g/cm^3, so it also holds the potential for scintillation application, especially under medium X-ray tube voltages.

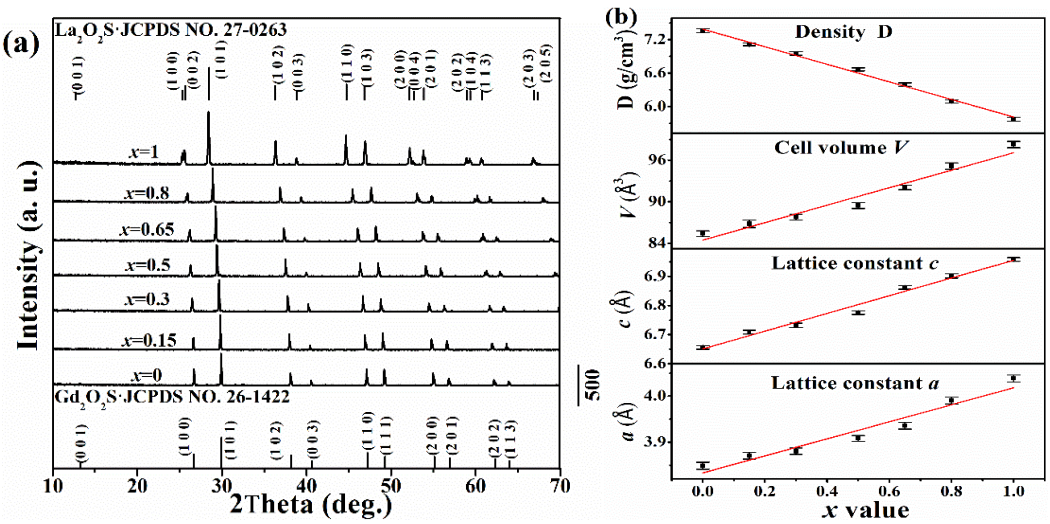

Fig. 5. XRD patterns (a) and lattice parameters, cell volume and theoretical density (b) of the GLOS:Pr^{3+} ceramics sintered at 1350 °C.

Fig. 6a shows the evolution of relative density as a function of sintering temperature for the series of GLOS:Pr^{3+} ceramics, where it can be clearly seen from the x = 0.8 and 1.0 compositions that La^{3+} dopiong faciliates densification, as also found from the results of dialotometry (Fig. 4). The ceramics have attained over 99% of their theoretical denisties at only 1300 °C and full densification (over 99.5%) was achieved at 1350 °C for all the compositions. Such temperatures are significantly lower than those reported for pressureless sintering of commerical powders or powders synthesized by other methods.

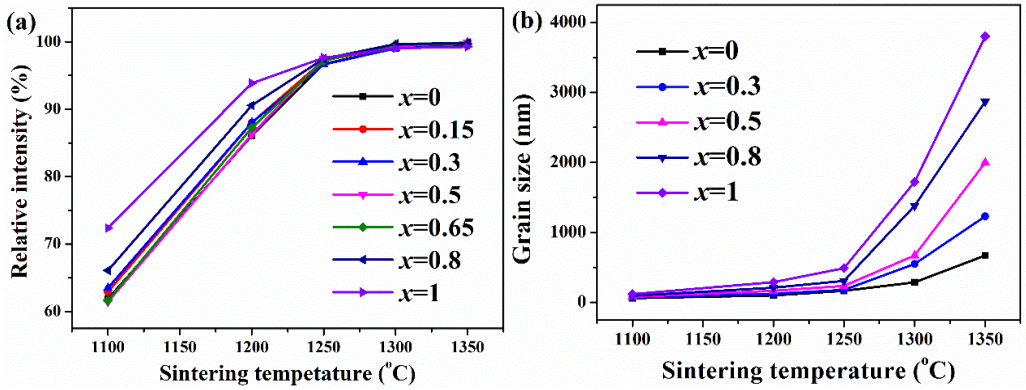

Fig. 6. Relative densities (a) and average grain sizes (b) of the GLOS:Pr^{3+} ceramics, as a function of the sintering temperature.

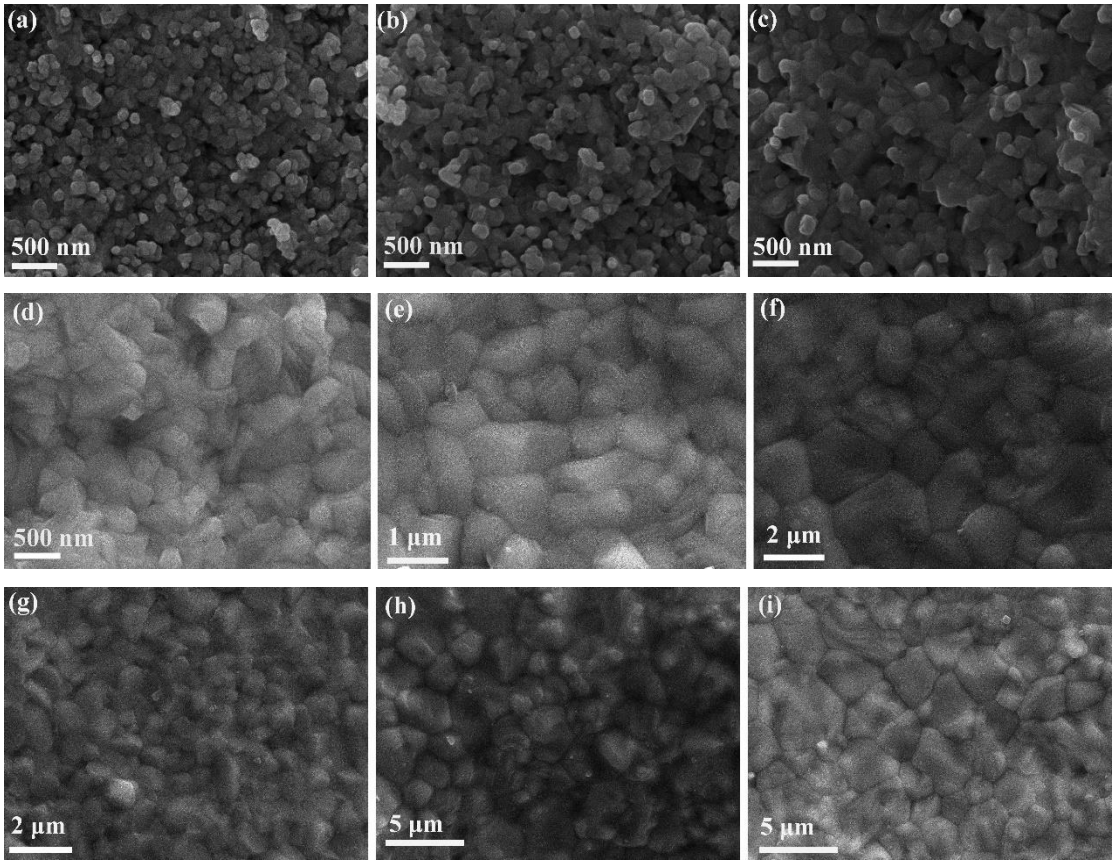

Fig. 7. FE-SEM micrographs of the GLOS:Pr^{3+} ceramics sintered at 1200 ºC (a, b, c), 1300 ºC (d, e, f) and 1350 ºC (g, h, i) for the x=0 (a, d, g), x=0.5 (b, e, h) and x=1.0 (c, f, i) compositions.

Fig. 7 shows the microstructures of the GLOS:Pr^{3+} ceramics sintered at 1200, 1300 and 1350 °C for the typical compositions of x = 0, 0.5 and 1.0. Pores can easily be observed in the three ceramics sintered at 1200 °C (Fig. 7a-c), since they have relative densities of ~86-93% (Fig. 6a), but the number of pores decreased significantly and the microstructures became much denser when x reached 1.0 (Fig. 7c), conforming to the higher relative density of this ceramic (Fig. 6a). Meanwhile, the average grain size of the ceramics increased from ~99 nm for x = 0 to ~167 nm for x = 0.5 and then to ~290 nm for x = 1.0 (Fig. 6b). Significant promotion of grain growth by a higher La^{3+} content was also confirmed from the microstructures of the ceramics sintered at 1300 and 1350 °C (Fig. 7) and from the average grain sizes shown in Fig. 6b, due to the aforesaid

lattice ionicity and lattice expansion reasons. The ceramic samples sintered at 1300 °C have very few pores (Fig. 7), conforming to their high degree of densification (Fig. 6a). Sintering at 1350 °C caused full densification, with pores hardly observable, and significant grain growth, and the x = 0, 0.5 and 1.0 compositions have their respective average grain sizes of ~0.67, 2.0, and 3.5 μm (Fig. 6b).

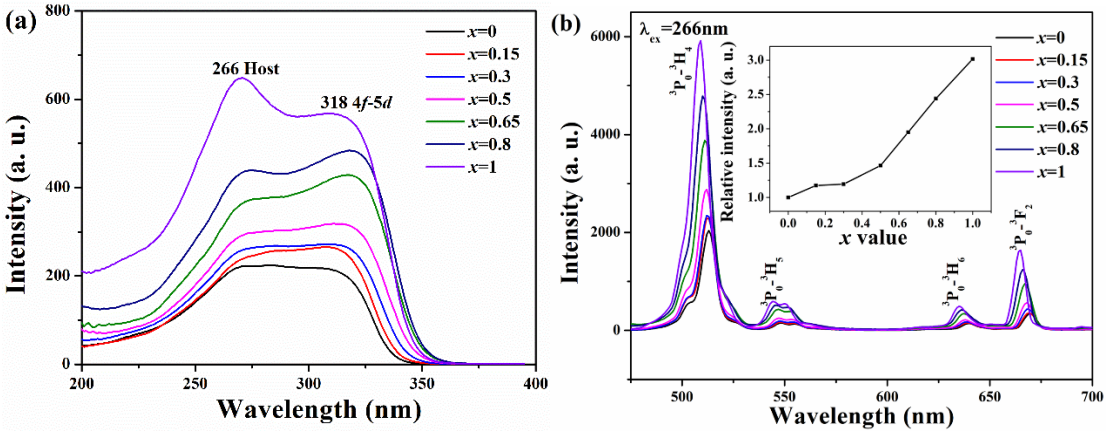

Fig. 8. Excitation (a) and emission (b) spectra of the GLOS:Pr^{3+} ceramics sintered at 1350 ºC, where the inset in (b) shows the relative intensity of the $^3P_0$-$^3H_4$ main emission.

Fig. 8a shows the excitation spectra of the series of GLOS:Pr^{3+} ceramics sintered at 1350 ºC, which were recorded by monitoring the peak wavelength (~509-512 nm) of the $^3P_0$-$^3H_4$ main emission of Pr^{3+}. It is seen that each sample showed a broad band up to ~375 nm, which arises from overlapping of host excitation (~266 nm; excitation of electrons from the valence band to the conduction band) [30] and the 4*f*-5*d* transition of Pr^{3+} (~318 nm) [31]. La_2O_2S absorbs UV light (up to ~325 nm, centered at ~255 nm) much stronger than Gd_2O_2S [5,32] and, therefore, the intensities of both the types of excitations gradually gained intensity with increasing La^{3+} content. The relative intensity of the two types of excitations would be affected by a number of factors, such as bandgap, which decreases for a higher La^{3+} content [32], the extent of lattice

distortion, which increases with increasing La^{3+} content up to $x = 0.5$ and then decreases up to $x = 1.0$, and the ionicity of the host lattice, which increases with increasing x. It is, however, difficult to differentiate the contribution of each factor. Fig. 8b shows the emission spectra of the GLOS:Pr^{3+} ceramics taken under 266 nm excitation, where it is seen that the Pr^{3+} activator exhibited its typical $^3P_0$-$^3H_4$ (~512 nm), $^3P_0$-$^3H_5$ (~547 nm), $^3P_0$-$^3H_6$ (~635 nm) and $^3P_0$-$^3F_2$ (~665 nm) transitions in each case, with the $^3P_0$-$^3H_4$ one being the most prominent. The emission peaks were gradually blue shifted with increasing La^{3+} content, and the $^3P_0$-$^3H_4$ main emission moved from 512 nm for $x = 0$ to 509 nm for $x = 1.0$. This is ascribable to the successively higher ionicity of the host lattice, which weakens crystal field splitting of the Pr^{3+} energy levels. It is also seen from the inset in Fig. 8b that the $^3P_0$-$^3H_4$ main emission steadily gained intensity at a higher La^{3+} content, conforming to the tendency observed from the host excitation band, and the La_2O_2S:Pr^{3+} (x=1.0) composition emits ~1.5 and 3.0 times as strong as the $x = 0.5$ and $x = 0$ ones, respectively.

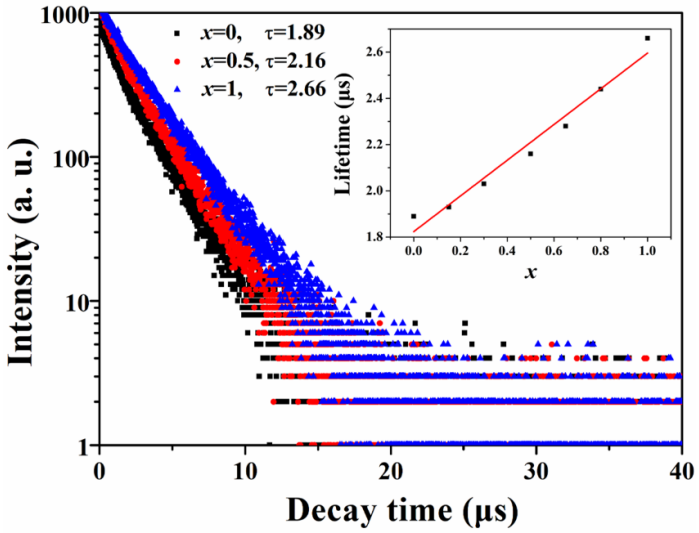

Fig. 9. Fluorescence decay curves for the three typical GLOS:Pr^{3+} ceramics sintered at 1350 °C.

Fig. 9 shows the fluorescence decay curves for the $^3P_0$-$^3H_4$ main emission of the GLOS:Pr^{3+} ceramics, with the three typical samples of x = 0, 0.5 and 1.0 for example. It is seen that the decay profiles are almost straight lines in each case. We thus applied equation $I = \exp(-t/\tau)$ to derive fluorescence lifetime τ, where I is relative emission intensity and t is decay time. Our fitting yielded τ values of ~1.89, 2.16 and 2.66 μs for the x = 0, 0.5 and 1.0 compositions, respectively, which basically agree with the ~2-5 μs reported for $Gd_2O_2S:Pr^{3+}$ scintillation ceramics [6]. Similar analysis was applied to the other ceramics and, as seen from the inset of Fig. 9, the fluorescence lifetime of Pr^{3+} tends to be linearly elongated by a higher La^{3+} content. This is primarily due to the gradually smaller refractive index by lattice expansion and lower theoretical density (Fig. 5b) of the material [33].

4. Conclusion

Calcining coprecipitated amorphous precursors in air and then in H_2 at 950 °C produced $[(Gd_{1-x}La_x)_{1.99}Pr]_2O_2S$ (GLOS:Pr^{3+}; x = 0-1.0) nanopowders of fine crystallite size, unimodal size distribution and high specific surface area. With such powders, GLOS:Pr^{3+} ceramics were fully densified via pressureless sintering in a flowing Ar/H_2 gas mixture at the very low temperature of 1350 °C for 4 h. It was found that La^{3+} doping may substantially promote densification and grain growth (~0.67-3.5 μm), enhance the intensity of the $^3P_0$-$^3H_4$ main emission (~510 nm) by three times, and tends to slightly elongate the fluorescence lifetime of the Pr^{3+} emission (~1.89-2.66 μs).

CRediT authorship contribution statement

Zhenqi Song: Formal analysis, Data curation, Writing – original draft. Fan Li, Sihan Feng, Zhiyuan Fan, Xuejiao Wang: Methodology, Formal analysis. Qi Zhu: Resources, Supervision. Ji-Guang Li: Writing – review & editing, Supervision.

Declaration of Competing Interest

The authors declare that they have no known competing financial interests or personal relationships that could have appeared to influence the work reported in this paper.

Acknowledgments

This work was partially supported by the Natural Science Foundation of China (No. 52172112, 52371057).

References

[1] Z.Y. Lin, S.C. Lv, Z.M. Yang, J.R. Qiu, S.F. Zhou, Structured scintillators for efficient radiation detection, Adv. Sci. 9 (2022) 2102439.

[2] C. Greskovich, S. Duclos, Ceramics scintillators, Annu. Rev. Mater. Sci. 27 (1997) 69-88.

[3] R. Nakamura, Improvements in the X-ray characteristics of Gd_2O_2S:Pr ceramic scintillators, J. Am. Ceram. Soc. 82 (1999) 2407-2410.

[4] J. Li, J.Y. Ding, X.Y. Huang, Rare earth doped Gd_2O_2S scintillation ceramics, J. Inorg. Mater. 36 (2021) 789-806.

[5] Z.Q. Song, F. Li, S.H. Feng, Z.Y. Pan, Q. Zhu, J-G. Li, Systematic synthesis of $(Gd_{1-x}La_x)_2O_2SO_4:Tb^{3+}$ and $(Gd_{1-x}La_x)_2O_2S:Tb^{3+}$ nanophosphors for remarkably enhanced luminescence, J. Am. Ceram. Soc.106 (2023) 7542-7555.

[6] H. Yamada, A. Suzuki, Y. Uchida, M. Yoshida, H. Yamamoto, A scintillator Gd_2O_2S:Pr,Ce,F for X-ray computed tomography, J. Electrochem. Soc. 136 (1989) 2713-2716 .

[7] S. Blahuta, B. Viana, A. Bessiere, E. Mattmann, B. LaCoure, Luminescence quenching processes in $Gd_2O_2S:Pr^{3+},Ce^{3+}$ scintillating ceramics, Opt. Mater. 33 (2011) 1514-1518.

[8] E.I. Gorokhova, V.A. Demidenko, S.B. Eron'ko, O.A. Khristich, S.B. Mikhrin, Spectrokinetic characteristics of Gd_2O_2S:Pr,Ce ceramics, J. Opt. Technol. 73 (2006) 130-137.

[9] C. Michail, I. Valais, I. Seferis, N. Kalyvas, S. David, G. Fountos, I. Kandarakis, Measurement of the luminescence properties of Gd_2O_2S:Pr,Ce,F powder scintillators under X-ray radiation, Radiat. Meas. 70 (2014) 59-64.

[10] W. Wang, H.M. Kou, S.P. Liu, Y. Shi, J. Li, Y.S. Li, X.Q. Feng, Y.B. Pan, J.K. Guo, Comparison of the optical and scintillation properties of Gd_2O_2S: Pr, Ce ceramics fabricated by hot pressing and pressureless sintering, Opt. Mater. 42 (2015) 199-203.

[11] L. Chen, Z.H. Bai, Q.S. Liu, Photoluminescence/cathodoluminescence properties and energy transfer mechanisms of fine-particle $Gd_2O_2S:Tb^{3+}$, RE^{3+} (RE=Dy, Eu) phosphor, J. Lumines. 267 (2024) 120343.

[12] E.I. Sal'nikova, YuG. Denisenko, A.S. Aleksandrovsky, I.E. Kolesnikov, E. Lähd eranta, P.O. Andreev, N.O. Azarapin, O.V. Andreev, S.A. Basova, A.V. Matigorov, Synthesis and optical properties RE_2O_2S:Ln (RE = La, Y; Ln =Ce, Eu, Dy, Er), J.

Solid. State. Chem. 279 (2019) 120964.

[13] P. Jiang, Z.P. Li, W. Lu, Y. Ma, W.H. Tian, The pH value control of morphology and luminescence properties of $Gd_2O_2S:Tb^{3+}$ phosphors, Materials.15 (2022) 646.

[14] Y.H. Song, H.P. You, Y.J. Huang, M. Yang, Y.H. Zheng, L.H. Zhang, N. Guo, Highly uniform and monodisperse $Gd_2O_2S:Ln^{3+}$(Ln=Eu, Tb) submicrospheres: solvothermal synthesis and luminescence properties, Inorg. Chem. 49 (2010) 11499-11504.

[15] G.Q. Wu, H.M. Qin, S.W. Feng, X.J. Tan, Z.H. Luo, Y.F. Liu, H.Z. Shao, J. Jiang, H.C. Jiang, Ultrafine Gd_2O_2S:Pr powders prepared via urea precipitation method using SO_2/SO_4^{2-} as sulfuration agent—A comparative study, Powder. Technol. 305 (2017) 382-388.

[16] X. Luo, W. Cao, Ethanol-assistant solution combustion method to prepare La_2O_2S:Yb,Pr nanometer phosphor, J. Alloys. Compd. 460 (2008) 529-534.

[17] Z.L. Fu, Y. Geng, H.W. Chen, S.H. Zhou, H.K. Yang, J.H. Jeong, Combustion synthesis and luminescent properties of the Eu^{3+}-doped yttrium oxysulfide nanocrystalline, Opt. Mater. 31 (2008) 58-62.

[18] J. Gu, Y. Ding, J.Ke, Y.W. Zhang, C.H. Yan, Controllable synthesis of monodispersed middle and heavy rare earth oxysulfide nanoplates based on the principals of HSAB theory, Acta. Chim. Sin. 71 (2013) 360-366.

[19] E.I. Gorokhova, G.V. Anan'eva, V.A. Demidenko, S.B. Eron'ko, E.A. Oreshchenko, O.A. Khristich, P.A. Rodnyi, Scintillation optical ceramics based on Gd_2O_2S doped with Pr, Tb, or Eu, J. Opt. Technol.79 (2012) 41-45.

[20] E.I. Gorokhova, V.A. Demidenko, S.B. Eron'ko, E.A. Oreshchenko, P.A. Rodnyi, S.B. Mikhrin, Luminescence and scintillation properties of Gd_2O_2S:Eu optical ceramic, J. Opt. Technol. 77 (2010) 50-58.

[21] Q. Liu , F. Wu , X.P. Chen , H.H. Chen , W. Wang , Y. Shi , X.Y. Li , X. Liu , T.F. Xie, J. Li, Fabrication of Gd_2O_2S:Pr scintillation ceramics from water-bath synthesized nanopowders, Opt. Mater.104 (2020) 109946.

[22] X.Y. Huang, J.Y. Ding, X. Liu, X.Y. Li, H.H. Chen, D.J. Hu, D.Y. Zhu, T.F. Xie, J.R. Zhou, X.F. Jiang, Z.J. Sun, J. Li, Fabrication of Gd_2O_2S:Tb scintillation ceramics from the uniformly doped nanopowder, Opt. Mater.117 (2021) 111192.

[23] W. Wang, Y.S. Li, H.M. Kou, S.P. Liu, W.P. Liu, Y. Shi, J. Li, X.Q. Feng, Y.B. Pan, J.K. Guo, Fabrication of Gd_2O_2S: Pr, Ce, F scintillation ceramics by pressureless sintering in nitrogen atmosphere, Int. J. Appl. Ceram. Technol. 12 (2015) E249-E255.

[24] W. Wang, Y.S. Li, H.M. Kou, S.P. Liu, H. Liu, Y. Shi, J. Li, X.Q. Feng, Y.B. Pan, J.K. Guo, Gd_2O_2S:Pr scintillation ceramics from powder synthesized by a novel carbothermal reduction method, J. Am. Ceram. Soc. 98 (2015) 2159-2164.

[25] S. Chatterjee, V. Shanker, P.K. Ghosh, Trapping parameters and kinetics in Gd_2O_2S: Tb phosphor, Solid. State. Commun. 80 (1991) 877-890.

[26] X.J. Wang, J-G. Li, M.S. Molokeev, X.J. Wang, W.G. Liu, Q. Zhu, Hydrothermal crystallization of a $Ln_2(OH)_4SO_4{\cdot}nH_2O$ layered compound for a wide range of Ln (Ln = La-Dy), thermolysis, and facile transformation into oxysulfate and oxysulfide phosphors, RSC. Adv.7 (2017) 13331-13339.

[27] X.J. Wang, M.S. Molokeev, Q. Zhu, J-G. Li, Controlled hydrothermal crystallization of anhydrous $Ln_2(OH)_4SO_4$ (Ln = Eu-Lu, Y) as a new family of layered rare earth metal hydroxides, Chem. Eur. J. 23 (2017) 16034-16043.

[28] L.E. Sobon, K.A. Wickersheim, R.A. Buchanan, R.V. Alves, Growth and properties of lanthanum oxysulfide crystals, J. Appl. Phys. 42 (1971) 3049-3053.

[29] R.D. Shannon, Revised effective ionic radii and systematic studies of inter-atomic distances in halides and chalcogenides, Acta. Crystallogr. A32 (1976) 751-767.

[30] M. Raukas, K.C. Mishra, C. Peters, P.C. Schmidt, K.H. Johnson, J. Choi, U Happek, Electronic structure and associated properties of $Gd_2O_2S:Tb^{3+}$, J. Lumines. 87-89 (2000) 980-982.

[31] G. Blasse, B.C. Grabmaier, Luminescent materials, Berlin: Springer-Verlag; 1994

[32] Z.Q. Luo, F.L, Q.Zhu, X.D. Sun, X.D. Li, J-G. Li, Sulfidization-free synthesis of well dispersed $(Gd,La)_2O_2S:Pr^{3+}$ nanopowders and the effect of La^{3+}on structure and luminescence, J. Mater. Res. Technol. 18 (2022) 4216-4227.

[33] G. Dantelle, R. Calderon-Villajos, C. Zaldo, C. Cascales, Nanoparticle coatings with efficient up-conversion properties, ACS. Appl. Mater. Interfaces. 6 (2014) 22483-22489.